

# Contributions of solar-wind induced potential sputtering to the lunar surface erosion rate and its exosphere

S.T. Alnussirat<sup>a,\*</sup>, A.F. Barghouty<sup>b</sup>, J.E. Edmunson<sup>c</sup>, M.S. Sabra<sup>d</sup>, D.L. Rickman<sup>c</sup>

<sup>a</sup> Department of Physics, University of Alabama in Huntsville, Huntsville, AL 35899, United States

<sup>b</sup> Astrophysics Office, NASA-Marshall Space Flight Center, Huntsville, AL 35812, United States

<sup>c</sup> Jacobs ESSCA Group, Marshall Space Flight Center, Huntsville, AL 35812, United States

<sup>d</sup> USRA Space Science Department, Marshall Space Flight Center, Huntsville, AL 35805, United States

## ARTICLE INFO

### Keywords:

Solar-wind sputtering  
Potential sputtering  
Erosion rate  
Sputtering timescale  
Lunar exosphere

## ABSTRACT

Sputtering of lunar regolith by solar-wind protons and heavy ions with kinetic energies of about 1 keV/amu is an important erosive process that affects the lunar surface and exosphere. It plays an important role in changing the chemical composition and thickness of the surface layer, and in introducing material into the exosphere. Kinetic sputtering is well modeled and understood, but understanding of mechanisms of potential sputtering has lagged behind. In this study we differentiate the contributions of potential sputtering from the standard (kinetic) sputtering in changing the chemical composition and erosion rate of the lunar surface. Also we study the contribution of potential sputtering in developing the lunar exosphere. Our results show that potential sputtering enhances the total characteristic sputtering erosion rate by about 44%, and reduces sputtering time scales by the same amount. Potential sputtering also introduces more material into the lunar exosphere.

## 1. Introduction

Space weathering is a term used to describe the interaction of the surface material, also known as regolith with space energetic particles and radiation. Surfaces of celestial bodies that lack atmospheres and global magnetic fields, like our Moon, are exposed to many space weathering factors. Examples include (1) micrometeorite bombardment, which results in melting and vaporizing of the regolith [1], (2) Galactic Cosmic rays (GCRs), which result in chemical changes in the regolith through nuclear reactions [2], and (3) Solar-Wind Particles (protons and heavy ions), which results in particles ejection [1]. With varied energy ranges and penetration depths, GCRs and solar-wind particles interact with the lunar regolith through many processes. The most important process is the atomic sputtering by solar-wind, which takes place at the top layers of the regolith and can change the chemical composition (stoichiometry), roughness, and thickness of the surface as well as yield material for the lunar atmosphere.

Sputtering is the removal of near-surface species (atoms, ions, or molecules) from a target by the impact of high energy particles (atoms or ions). When an energetic particle imparts a target atom energy greater than the target's surface binding energy, the atom is likely to be sputtered. The sputtering efficiency of a surface is characterized by the "sputtering yield", which is defined as the mean number of the

sputtered target atoms per incident ion.

Ions that are singly charged and have kinetic energies in the keV range (like solar-wind protons) will mainly interact with the target atoms via binary collisions [3]. The kinetic energy and momentum of an incident particle is transferred to a target atom, causing radiation damage and ejection of atoms and/or ions from the target; this is known as "kinetic sputtering" (knock-on sputtering). The situation is completely different for multi-charged ions (like the solar-wind heavy ions), which are characterized by their high charge state and potential energy. While interacting with the surface, the multi-charged ions liberate and deposit this potential energy within a very small area (1 nm<sup>2</sup>) in a very short time (100 fs) [4]. This liberation and deposition always leads to nonlinear excitation processes, such as hollow atom formation or removal [5]. Ejection of target atoms by slow multi-charged ions impact is called potential sputtering. Multi-charged ion induced processes take place more effectively in insulators, because of the reduced electron mobility and fast electron removal from the target [6].

[7] studied the elemental changes of the lunar regolith due to kinetic and potential sputtering by solar-wind protons and heavy ions. In their work they used KREEP simulant to model the lunar regolith, which is a material composed of potassium, (K), rare Earth elements, (REE), and phosphorus, (P). They reported that potential sputtering has a significant effect on changing the chemical composition of the

\* Corresponding author.

E-mail address: [stn0003@uah.edu](mailto:stn0003@uah.edu) (S.T. Alnussirat).

regolith. To support their finding, we used in this study the JSC-1A AGGL simulant for lunar regolith and estimated the elemental changes of the regolith elements due to kinetic and potential sputtering. We have extended their study by estimating the surface erosion rate, characteristic time scale, and the density of elements provided by sputtering into the lunar exosphere.

In the following section we discuss solar-wind constituents and flux, and composition of the JSC-1A AGGL simulant. In Section 3 we use a non-equilibrium model for sputtering to calculate elemental changes in a target due to incident particles, and study the effect of kinetic and potential sputtering. The effects of geometrical and gravitational factors in the sputtering process are discussed in Section 4. In Section 5 we calculate the erosion rate and the characteristic sputtering time scale of the lunar surface. Finally in Section 6 we calculate the density of the sputtered atoms that will contribute in developing the lunar exosphere.

## 2. Solar-wind flux, the JSC-1A AGGL simulant, and the lunar exosphere

Typical solar-wind fluxes are of the order  $10^8$  ion/cm<sup>2</sup>s, with energies in the range 350–1200 eV/amu. About 93% of the flux is protons, and the other 7% are light and heavy ions (He, O, C, Ne, N, Si, Mg, S, Fe, and Ar) (see Table 1), which are characterized by charge state and potential energy [8,9]. Actual lunar regolith material is composed of oxides in the form of soil grains surrounded by amorphous melt layers, called rims [10]. Kinetic and potential sputtering by solar-wind protons and heavy ions take place effectively in the lunar regolith material. The impact on lunar regolith by singly charged ions (e.g., protons) will result in kinetic sputtering, while the multi-charged ions (e.g., solar-wind light and heavy ions) will result in both kinetic and potential sputtering. The JSC-1A AGGL is a lunar regolith simulant developed by the company Orbitec.<sup>1</sup> This simulant is composed mostly of oxides of the elements given in Table 2. [11] studied the JSC-1A AGGL elemental chemical composition experimentally using X-ray photoelectron spectroscopy (XPS). The elemental composition of JSC-1A AGGL is an averaged between cores and rims elements.

The lunar exosphere composition has been studied and identified by different instruments [12–20]. The sources of elements in the lunar exosphere are mainly atomic sputtering by solar-winds, vaporization by micrometeorites impact and photon stimulated desorption [21,22]. In this work we focus on the sputtering process, and we estimate the contribution of potential sputtering as an additional source.

## 3. Modeling of the regolith elemental changes

The two erosive processes, solar-wind induced sputtering and micro-meteoritic impacts, can be coupled through an important characteristic property; the time scale. The erosion process time scale due to micro-meteoritic impacts is believed to be on the order of thousands of years [23,24], while for the solar-wind it is expected to be shorter [23,7]. [23] proposed a non-equilibrium model to study elemental changes in a target, which is the same model used by [7] to study the elemental changes in the lunar regolith KREEP. The elemental change of element  $i$  in a multi-element target is given by,

$$\frac{dC_i}{dt} = \frac{1}{\tau} \left( -C_i \sum_j Y_{ij} f_j + C_i^b \sum_{kj} C_k Y_{kij} f_j \right) \quad (1)$$

where  $C_i$  is the abundance of element  $i$  in the target,  $C_i^b$  is the fractional abundance of element  $i$  in the target bulk,  $Y_{ij}$  is the yield of element  $i$  by solar-wind ion  $j$ ,  $f_j$  is the fraction of solar-wind  $j$  in the solar-wind flux, and  $\tau$  is a constant that has the dimension of time defined as:

**Table 1**  
Charge state<sup>a</sup>, and fraction<sup>b</sup> in the solar-wind flux.

| Ion | Charge State                    | Fraction             |
|-----|---------------------------------|----------------------|
| H   | 1 <sup>+</sup>                  | 0.93                 |
| He  | 2 <sup>+</sup>                  | 0.04                 |
| O   | 6 <sup>+</sup> –8 <sup>+</sup>  | $7 \times 10^{-4}$   |
| C   | 4 <sup>+</sup> –6 <sup>+</sup>  | $3 \times 10^{-4}$   |
| Ne  | 7 <sup>+</sup> –9 <sup>+</sup>  | $3 \times 10^{-4}$   |
| N   | 5 <sup>+</sup> –7 <sup>+</sup>  | $1 \times 10^{-4}$   |
| Si  | 6 <sup>+</sup> –12 <sup>+</sup> | $3 \times 10^{-5}$   |
| Mg  | 7 <sup>+</sup> –10 <sup>+</sup> | $3 \times 10^{-5}$   |
| S   | 6 <sup>+</sup> –11 <sup>+</sup> | $1.6 \times 10^{-5}$ |
| Fe  | 7 <sup>+</sup> –14 <sup>+</sup> | $8 \times 10^{-6}$   |
| Ar  | 7 <sup>+</sup> –10 <sup>+</sup> | $4 \times 10^{-6}$   |

<sup>a</sup> From [8]

<sup>b</sup> From [9]

**Table 2**  
XPS analysis of JCS-1A AGGL sample surface composition.<sup>c</sup>

| Element        | % Atomic fraction |
|----------------|-------------------|
| C <sup>d</sup> | 2.3               |
| O              | 55.6              |
| Si             | 19.5              |
| Al             | 8.4               |
| Fe             | 1.4               |
| Ca             | 4.3               |
| Mg             | 3.9               |
| Ti             | 0.4               |
| Na             | 3.3               |
| P              | 0.3               |
| K              | 0.3               |
| Cr             | 0.1               |
| F              | 0.1               |

<sup>c</sup> From [11]

<sup>d</sup> The source of carbon in the JSC sample is a carbon tape used in the experiment [11].

$$\tau = \frac{h}{j \langle Y \rangle a^3} \quad (2)$$

where  $j = 10^8$  cm<sup>−2</sup> s<sup>−1</sup> is the solar-wind flux,  $\langle Y \rangle$  is the total sputtering yield (see Section 4),  $a = 2.23 \times 10^{-8}$  cm is the average enter-atomic spacing, and  $h = 300$  Å is the ion penetration depth.

To study the effect of potential sputtering, we begin by calculating the changes in the elemental abundance for JSC-1A AGGL. We assume that the dynamics of the sputtering process is only due to kinetic sputtering and ignore the effect of the potential sputtering. Applying Eq. (1) on JSC-1A AGGL elements, given in Table 1, we obtain a set of 13 coupled differential equations, with the initial condition  $C_i(0) = C_i^b$ . The equations are solved using the numerical method of lines [25]. The kinetic sputtering yields  $Y_{ij}$  are calculated using the simulation package SRIM (The Stopping and Range of Ions in Matter) [26], where the default values for the density, lattice, displacement, and surface binding energies of the target are used in the simulation. The energy of the solar-wind ions is set to 1 keV/amu at normal incident.

Fig. 1 shows the calculated changes in the elemental abundance of JSC-1A AGGL due to the solar-wind protons. These changes approach a steady state for times after 300  $\tau$ . Fig. 2 shows the calculated changes in the elemental abundance of JSC-1A AGGL due to the solar-wind protons and heavy ions. These changes approach a steady state for times after 200  $\tau$ . Steady-state compositional changes are summarized in Table 3, where the sign + (−) means enhancement (reduction).

The expected compositional changes, shortened time scale, and overall enhancement in the sputtering yield (due to inclusion of heavy ions) are all consistent with the KREEP results of [7].

In light of the experimental data of [11,7] have shown that

<sup>1</sup> www.orbitec.com.

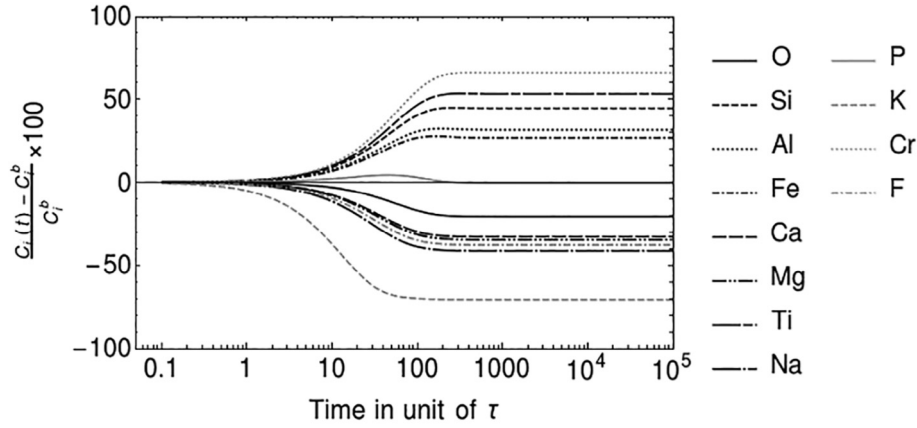


Fig. 1. Calculated changes in the elemental composition of a JSC-1A AGGL surface as a function of time due to the kinetic sputtering of the solar-wind protons.

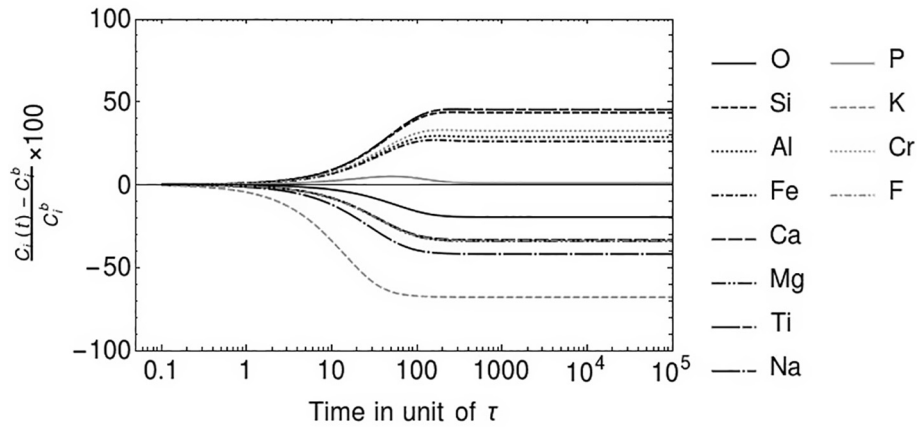


Fig. 2. Calculated changes in the elemental composition of a JSC-1A AGGL surface as a function of time due to the kinetic sputtering of the solar-wind protons and heavy ions.

Table 3

Steady-state changes in the composition of JSC-1A AGGL due to kinetic-sputtering of solar-wind protons, and protons and heavy ions (HIs).

| Element | Protons | Protons and HIs (kinetic) | Protons and HIs (total) |
|---------|---------|---------------------------|-------------------------|
| O       | -20     | -19                       | -41                     |
| Si      | +54     | +55                       | +75                     |
| Al      | +31     | +29                       | +58                     |
| Fe      | +27     | +28                       | +54                     |
| Ca      | -32     | -32                       | -18                     |
| Mg      | -34     | -32                       | -19                     |
| Ti      | +53     | +45                       | +78                     |
| Na      | -41     | -41                       | -29                     |
| P       | 0       | 0                         | +24                     |
| K       | -70     | -69                       | -61                     |
| Cr      | +65     | +32                       | +61                     |
| F       | -39     | -33                       | -19                     |

including potential sputtering enhanced the sputtering process for KREEP significantly. To calculate the yields due to potential sputtering, [7] have adopted Tona model [27]. In this model the sputtering yield of element  $i$  due to the potential energy of ion  $j$  is given by,

$$Y_{ij}^{pot} = \alpha_i \varepsilon_j^{\beta_i} \quad (3)$$

with

$$\varepsilon_j = \sum_n E_n - E_1 \quad (4)$$

where  $E_1$  and  $E_n$  are the first and  $n$ th ionization energy for the solar-wind ion  $j$ , and  $\alpha_i$  and  $\beta_i$  are parameters depending on element  $i$ . The

total sputtering yield of element  $i$  is,

$$Y_i^{tot} = Y_i^{kin} + Y_i^{pot} \quad (5)$$

To calculate the potential sputtering for each element in JSC-1A AGGL, we have used, for oxygen sputtered atoms,  $\alpha_{oxygen} = 3.12$ , and  $\beta_{oxygen} = 0.57$ , while all other elements of JSC-1A AGGL have zero  $\alpha_i$  and  $\beta_i$  [7].

Fig. 3 shows the changes in the elemental abundance of JSC-1A AGGL, due to the solar-wind protons and heavy ions, including both kinetic and potential sputtering. These changes approach the steady state for times less than  $200 \tau$ . Steady state elemental changes are summarized in Table 3.

These results show that the potential sputtering process has significant effects and plays an important role in changing the surface-chemical composition. One can see from Table 3 that the reduction in O is 19% due to the kinetic sputtering and 41% due to the total sputtering (both kinetic and potential), (32% vs. 18%) for Ca, (32% vs. 19%) for Mg, (69% vs. 61%) for K and (33% vs. 19%) for F. On the other hand, the enhancement in Si is (55% vs. 75%), (29% vs. 58%) for Al. (28% vs. 54%) for Fe, (45% vs. 78%) for Ti and (32% vs. 61%) for Cr. All such changes are consistent with those calculated earlier for the KREEP surfaces as outlined in [7]. We note, however, these steady state elemental changes can be affected by other processes and become invalid if the time scale of these other processes is comparable to the sputtering time scale. Also, a mix of elements like the JSC-1A AGGL and an actual regolith can be different in density and surface binding energies. These differences will affect the sputtering process. However, the importance of potential sputtering is expected to be the same in a mixture of elements like the JSC-1A AGGL and an actual regolith. Likewise, we expect

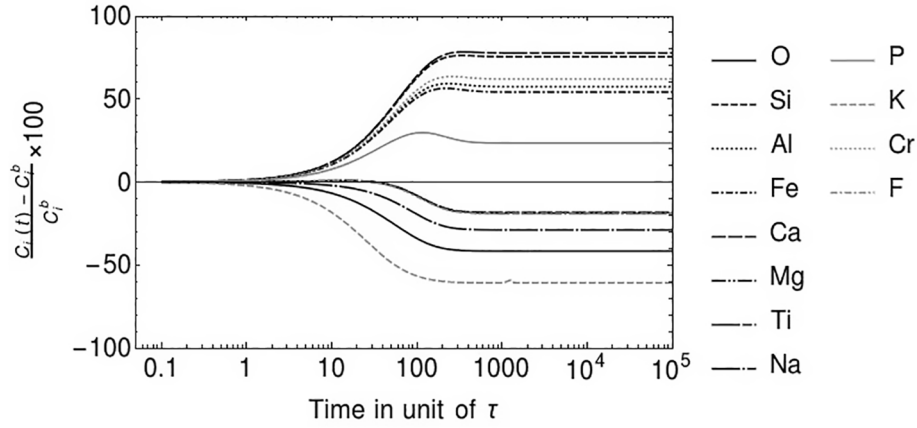


Fig. 3. Calculated changes in the elemental composition of a JSC-1A AGGL surface as a function of time due to both kinetic and potential sputtering of the solar-wind protons and heavy ions (HIs).

to see a significant effect on the erosion rate and sputtering time scale due to potential sputtering, which we address next.

#### 4. Geometrical and gravitational factors

There are two possible outcomes for the ejected atoms, either to gravitationally escape from the Moon or to return back to the surface. These outcomes are determined by gravitational and geometrical factors, but most importantly by the energy distribution of the ejecta [23].

The effect of the gravitational factor can be estimated from the energy distribution of the sputtered atoms. On the other hand, the effect of the geometrical factor can be estimated from the total sputtering yield, which depends on the ion's angle of incidence. Both factors are important to estimate the surface erosion rate and sputtering time scale.

For the geometrical factor effect we have used SRIM [26] to estimate the kinetic sputtering yields at different incident angles (between  $0^\circ$  and  $90^\circ$ ). Potential sputtering is expected to increase the sputtering yield as shown in Section 2. The total sputtering yield can be estimated by adding the potential sputtering yields (calculated from Eq. (2)) with the kinetic sputtering yields. For simplicity, potential sputtering is assumed to be independent of the angle of incidence of the ion.

Fig. 4 shows the kinetic and total sputtering coefficient as a function of the ion's incidence angles.

The coefficient of kinetic sputtering due to protons and heavy ions

$Y^{kin}(\theta)$  can be approximated using,

$$Y^{kin}(\theta) = 0.0174 + 1.051\theta^4 - 5.426\theta^5 + 11.251\theta^6 - 11.431\theta^7 + 5.686\theta^8 - 1.108\theta^9 \quad (6)$$

The coefficient of total sputtering  $Y^{total}(\theta)$  can be approximated using,

$$Y^{tot}(\theta) = 0.0333 + 1.051\theta^4 - 5.426\theta^5 + 11.251\theta^6 - 11.431\theta^7 + 5.686\theta^8 - 1.108\theta^9 \quad (7)$$

where  $\theta$  is the ion angle of incidence in radians. The total sputtering yield ( $Y$ ) averaged over all angles of incidence, can be estimated by,

$$\langle Y \rangle = \frac{\int_0^{\pi/2} Y(\theta) \cos(\theta) \sin(\theta) d\theta}{\int_0^{\pi/2} \cos(\theta) \sin(\theta) d\theta} \quad (8)$$

Averaging over all angles of incidence takes into account both the directionality of the solar-wind and the local roughness of the regolith. The value of  $\langle Y \rangle$  is 0.036 for kinetic sputtering. However,  $\langle Y \rangle$  is 0.052 for total sputtering. Therefore, potential sputtering enhances the sputtering yield by 44%.

To estimate the effect of the lunar gravitational field, an energy distribution of the sputtered atoms is required. Sputtered atoms with energy greater than the escape energy, will leave the Moon. The experimental studies of energy distributions of sputtered atoms agree with Thompson's model [28] for singly charged ions for kinetic energies of

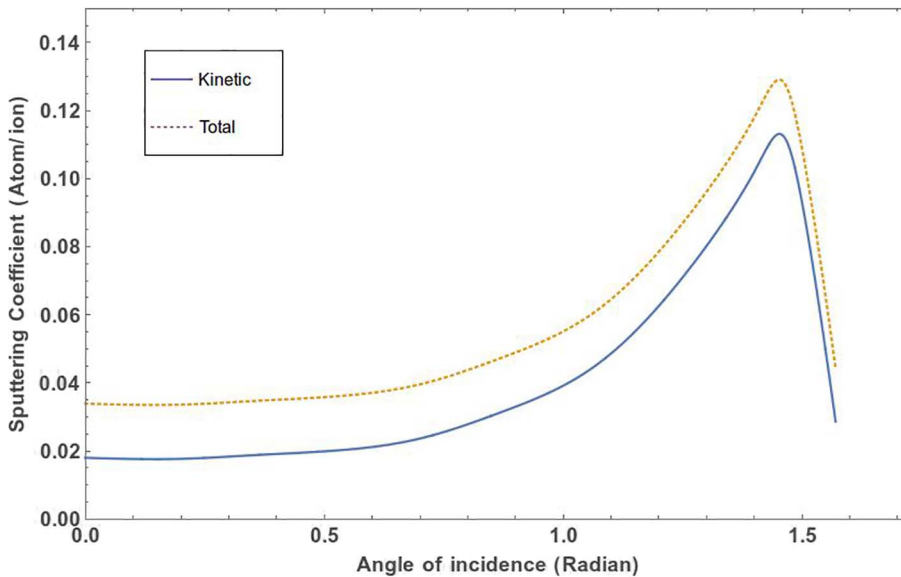


Fig. 4. Protons and heavy ions induced kinetic and total sputtering coefficients  $Y$  as functions of the angle of incidence  $\theta$ .

about 1 keV [29]. Thompson's model is given by [28]:

$$f(E)dE = C \frac{E}{(E+U)^3} dE \quad (9)$$

where  $C$  is a normalization constant,  $E$  is the energy of the sputtered atom, and  $U$  is the atom target surface binding energy, both in units of eV. This behavior is obviously due to the kinetic sputtering, since there are no potential sputtering effects in the case of singly charged ions. [23] studied the kinetic sputtering of lunar regolith by solar wind ions. The energy distribution of the sputtered atoms according to that study supports Thompson's model. However, for multi-charged ions, we will assume the energy distribution of the sputtered atoms to be broad, based on the experimental work in [30].

We estimate the energy distribution of the sputtered atoms as the convolution of two distribution functions (kinetic  $f^{kin}(E)$  and potential  $f^{pot}(E)$ ) as follows: we assume that the total energy ( $E^{tot}$ ) of the sputtered atoms is a random variable,

$$E^{tot} = AE^{kin} + BE^{pot} \quad (10)$$

where

$$A = \frac{Y^{kin}}{Y^{kin} + Y^{pot}} \quad (11)$$

$$B = \frac{Y^{pot}}{Y^{kin} + Y^{pot}} \quad (12)$$

A representative fit of  $f^{kin}$  suggests,

$$f^{kin}(x) = \left( \frac{1}{e^{a_1(x-b_1)} + 1} \right) \left( \frac{1}{e^{a_1(-x-b_1)} + 1} \right) \quad (13)$$

and we assume  $f^{pot}$  to be broad and having same structure as,  $f^{kin}$

$$f^{pot}(x) = \left( \frac{1}{e^{a_2(x-b_2)} + 1} \right) \left( \frac{1}{e^{a_2(-x-b_2)} + 1} \right) \quad (14)$$

where  $x = \text{Log}_{10}(\frac{E}{E_0})$  and  $a_1, b_1, a_2$ , and  $b_2$  are dimensionless fixed parameters, and  $E_0 = 1$  eV. Here we are assuming that the atom is sputtered due to either kinetic or potential mechanisms according to their respective weights ( $A$  and  $B$ ) as defined by the yields. We assume the weights  $A$  and  $B$  to be equals and equal to (0.5). Based on the convolution of the two distributions  $f^{kin}$  and  $f^{pot}$ , the total energy distribution can be written as:

$$f^T(E) = \int_0^\infty f^{kin}(E)f^{pot}(E-E')dE' \quad (15)$$

Fig. 5 shows the three distributions using  $a_1 = 2.85, b_1 = 0.5, a_2 = 5.5$  and  $b_2 = 2$ . Please note that Eq. 14 is an assumed energy distribution function of the sputtered atoms by potential sputtering. To get better approximation of the sputtering erosion rate and time scale, an accurate experimental energy distribution function is needed for regolith like material.

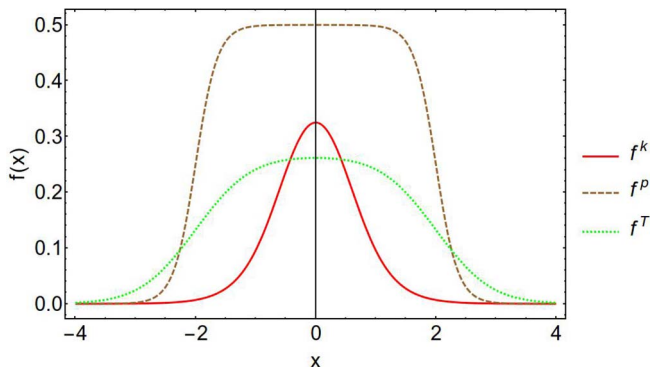


Fig. 5. Assumed energy distributions of the sputtered atoms.

Table 4

Escape energies  $E_e$  and the fraction of the sputtered atoms that will leave the gravitational field of the Moon  $\delta_l$ , for each JSC element.

| Element | $E_e$ (eV) | $\delta_l$ |
|---------|------------|------------|
| O       | 0.47       | 0.71       |
| Si      | 0.822      | 0.655      |
| Al      | 0.792      | 0.659      |
| Fe      | 1.644      | 0.581      |
| Ca      | 1.17       | 0.617      |
| Mg      | 0.704      | 0.67       |
| Ti      | 1.409      | 0.598      |
| Na      | 0.6698     | 0.677      |
| P       | 0.9025     | 0.645      |
| K       | 1.1392     | 0.62       |
| Cr      | 1.515      | 0.589      |
| F       | 0.553      | 0.697      |

Table 5

The surface density ( $\text{cm}^{-3}$ ) of each element due to kinetic sputtering  $\rho$  (kinetic), total sputtering  $\rho$  (total), and upper limit observations by the Lunar Reconnaissance Orbiter (LRO) [16].

| Element | $\rho$ kinetic       | $\rho$ total | LRO upper limit <sup>†</sup> |
|---------|----------------------|--------------|------------------------------|
| O       | 17.3                 | 64.5         | 5.4                          |
| Si      | 1.54                 | 5.47         | 0.9                          |
| Al      | 0.33                 | 1.99         | 1.1                          |
| Fe      | 0.012                | 0.41         | 45                           |
| Ca      | 0.21                 | 1.25         | 16                           |
| Mg      | 0.13                 | 0.86         | 3.4                          |
| Ti      | $8.7 \times 10^{-4}$ | 0.11         | *                            |
| Na      | 0.11                 | 0.72         | *                            |
| P       | $5.2 \times 10^{-4}$ | 0.06         | 4.2                          |
| K       | $1.6 \times 10^{-3}$ | 0.073        | *                            |
| Cr      | $5.7 \times 10^{-5}$ | 0.03         | *                            |
| F       | $5.8 \times 10^{-4}$ | 0.02         | *                            |

\* No reported values.

<sup>†</sup> From Table 1 in [16].

## 5. Modeling of the surface erosion rate and sputtering time scale

Based on the energy distribution in Fig. 5 and assuming the lunar surface materials as powder, the erosion rate and sputtering time scale can be estimated as the following, the erosion rate  $V$  is given by,

$$V = j\langle Y \rangle \delta_l \omega \quad (16)$$

and the sputtering time scale  $\tau$  is given by,

$$\tau = \frac{h}{j\langle Y \rangle a^3} \quad (17)$$

where  $\omega = 10^{23} \text{ cm}^{-3}$  is the atomic volume in a solid substance. The fraction of sputtered atoms that have kinetic energies greater than the escape energy  $\delta_l$  is given by,

$$\delta_l = \frac{\int_{E_e}^\infty f^T(E) dE}{\int_0^\infty f^T(E) dE} \quad (18)$$

The fraction of sputtered atoms that will leave the surface were calculated and are summarized in Table 4.

The average fraction of sputtered atoms that will leave the gravitational field of the Moon is  $\delta_l = 0.668$ . The erosion rate due to sputtering is found to be  $V_{kin} = 0.076 \text{ Å/year}$  for kinetic sputtering, while  $V_{tot} = 0.11 \text{ Å/year}$  for both kinetic and potential sputtering.

$V = (0.13-0.2) \text{ Å/year}$  is reported by [23] due to kinetic sputtering induced by solar-wind protons and heavy ions. The lower limit is consistent with our total erosion rate.

Another erosion mechanism important to regolith is due to micro-meteorite impacts. [31] estimated the vaporization rate due to micro-meteorites to be  $0.1 \text{ Å/year}$  assuming that all the vapor will leave the



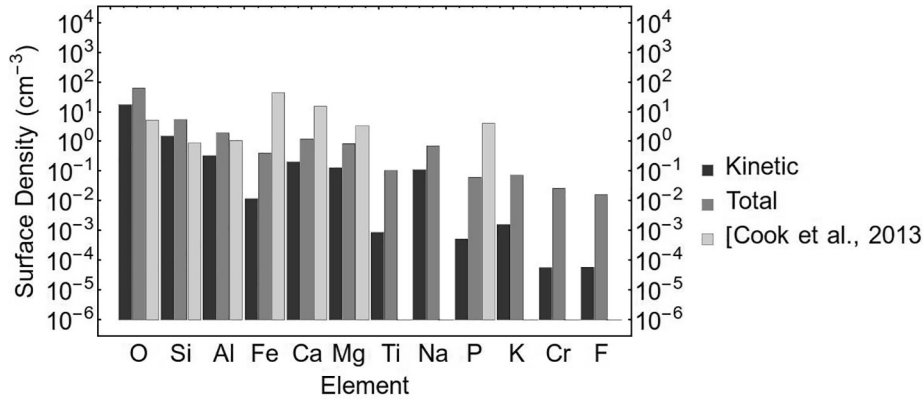


Fig. 6. Comparison of the calculated surface density due to sputtering with newer upper limits observations [16].

surface. This indicates that sputtering and vaporization contribute equally to the erosion rate. The same study suggest that most of the vapor will re-condense onto the lunar surface. Both results suggest that the solar-wind induced erosion may be as (or more) important an effect than micrometeorites impact.

From Eq. (16) the sputtering time scale due to kinetic sputtering is estimated to be about 2300 years. This time will be shortened by 44% to about 1600 years due to the inclusion of potential sputtering.

## 6. Contribution of sputtering to the exosphere

As shown in Section 5, potential sputtering will enhance the erosion rate, and as a consequence eject more atoms into the exosphere. Here we calculate the flux and surface density of neutral elements that results from sputtering. In these calculations we do not consider any transport of the sputtered atoms. Hence, we consider the calculated densities as characteristic densities. The flux of the sputtered atoms of element  $i$  ( $f_i$ ), in  $\text{cm}^{-2} \text{s}^{-1}$  is given by,

$$f_i = j C_i \langle Y_i \rangle \quad (19)$$

where  $\langle Y_i \rangle$  is the total sputtering yield of element  $i$  averaged over all angles of incidence. Here we consider potential sputtering to enhance the sputtering yield of all JSC-1A AGGL elements; we use  $\alpha = 3.12$  and  $\beta = 0.57$  for all elements.

The surface density  $\rho_i (\text{cm}^{-3})$  of element  $i$  in the exosphere can be calculated by dividing the flux by the average velocity of the sputtered atoms of that element,

$$\rho_i = \frac{f_i}{\langle v_i \rangle} \quad (20)$$

The average velocities are calculated from the energy distribution functions of Section 4.

Table 5 shows the calculated surface density of the JSC-1A AGGL elements due to kinetic and potential sputtering induced by solar-wind protons and heavy ions. These calculated surface densities are compared with upper limit observations from the Lunar Reconnaissance Orbiter (LRO) [16].

It can be seen clearly from Table 5 that potential sputtering enhances the surface density of the exosphere elements. Fig. 6 shows the density in  $\text{cm}^{-3}$  of each element compared to the LRO upper limits [16]. By comparing the calculated surface densities with the LRO upper limits in Fig. 6, our calculations suggest that sputtering is a significant source of some elements in the lunar exosphere. The calculated surface density of O, Si, and Al due to kinetic and total sputtering exceed the upper limit observations reported by LRO [16]. Which suggests that there might be some mechanisms that deplete these elements, such as the ionization of the sputtered O, Si, and Al atoms in the exosphere by the solar-wind impact. While other elements (Fe, Ca, Mg, and P) are consistent with the LRO upper limits.

## 7. Conclusions

In a non-equilibrium model we calculate the erosion rate and sputtering yield due to the interaction of solar-wind protons and heavy ions with lunar regolith. We used the JSC-1A AGGL simulant as a target material. We included both kinetic and potential sputtering, taking geometrical and gravitational effects into account, and used estimates of the sputtered atoms energy distributions. Our study was designed to isolate and quantify the contribution of potential sputtering.

Our study has shown that atomic sputtering of lunar regolith by solar wind protons and heavy ions has a significant effect in changing the chemical composition of lunar regolith. The total kinetic sputtering yield is estimated to be 0.036 atom/ion due to protons and heavy ions, while potential sputtering enhanced this yield to 0.052 atom/ion.

The erosion rate is found to increase from 0.076 Å/year to 0.11 Å/year due to the inclusion of potential sputtering, which suggests that atomic sputtering (by solar-wind protons and heavy ions) and vaporization (by micrometeorites) both contribute significantly to the erosion process. Potential sputtering is also found to shorten the characteristic sputtering time scale from about 2300 years to about 1600 years.

This study has demonstrated that potential sputtering due to solar-wind heavy ions enhance the surface density of some elements in the lunar exosphere. However, to explain the observed surface densities of some elements (e.g., O, Si, and Al), the inclusion of depletion mechanism(s) are needed. While other elements (Fe, Ca, Mg, and P) are consistent with the LRO upper limit observations. Other mechanisms like impacts by micrometeorites should be taken into account to understand the lunar exosphere composition.

The energy distribution of the sputtered atoms is estimated via the convolution of two functions. An experimental estimation of such distribution still not in hand and may affect the calculations of the erosion rate and sputtering time scale. Our study has demonstrated the critical role of potential sputtering in setting both the erosion rate and the characteristic time-scale of the sputtering of solar-wind protons and heavy ions on lunar regolith material.

## Acknowledgement

This work has been supported in part by NASA's Lunar Science and Advanced Research (LASER) program Grant No. NNN12AU21I at Marshall Space Flight Center. We also thank Dr. Fred Meyer (Oak Ridge National Laboratory) for his guidance and support.

## References

- [1] B. Hapke, W. Cassidy, E. Wells, Effects of vapor-phase deposition processes on the optical, chemical, and magnetic properties of the lunar regolith, *Moon* 13 (1–3) (1975) 339–353.
- [2] K. Kudela, M. Storini, M.Y. Hofer, A. Belov, Cosmic rays in relation to space weather, *Cosmic Rays and Earth*, Springer, 2000, pp. 153–174.

- [3] J.F. Ziegler, J. Biersack, U. Littmark, The stopping and range of ions in solids, vol. 1, New York, 1985.
- [4] F. Aumayr, H. Winter, Potential sputtering, *Philos Trans R Soc London Ser A: Math Phys Eng Sci* 362 (1814) (2004) 77–102.
- [5] P. Sigmund, Fundamental processes in sputtering of atoms and molecules (SPUT92): symposium on the occasion of the 250th anniversary of the Royal Danish Academy of Sciences and Letters, Copenhagen, 30 August–4 September, 1992: invited reviews, vol. 43, Kongelige Danske videnskabernes selskab, 1993.
- [6] A. Arnau, F. Aumayr, P. Echenique, M. Grether, W. Heiland, J. Limburg, R. Morgenstern, P. Roncin, S. Schippers, R. Schuch, et al., Interaction of slow multicharged ions with solid surfaces, *Surf. Sci. Rep.* 27 (4) (1997) 113–239.
- [7] A. Barghouty, F.W. Meyer, P.R. Harris, J. Adams Jr, Solar-wind protons and heavy ions sputtering of lunar surface materials, *Nucl. Instrum. Methods Phys. Res., Sect. B* 269 (11) (2011) 1310–1315.
- [8] R. Von Steiger, N. Schwadron, L. Fisk, J. Geiss, G. Gloeckler, S. Hefti, B. Wilken, R. Wimmer-Schweingruber, T. Zurbuchen, Composition of quasi-stationary solar wind flows from ulysses/solar wind ion composition spectrometer, *J. Geophys. Res.* 105 (A12) (2000) 27217–27238.
- [9] S. Bame, J. Asbridge, W. Feldman, M. Montgomery, P. Kearney, Solar wind heavy ion abundances, *Sol. Phys.* 43 (2) (1975) 463–473.
- [10] L.P. Keller, D.S. McKay, The nature and origin of rims on lunar soil grains, *Geochim. Cosmochim. Acta* 61 (11) (1997) 2331–2341.
- [11] F. Meyer, P. Harris, C. Taylor, H. Meyer III, A. Barghouty, J. Adams, Sputtering of lunar regolith simulant by protons and singly and multicharged ar ions at solar wind energies, *Nucl. Instrum. Methods Phys. Res., Sect. B* 269 (11) (2011) 1316–1320.
- [12] A. Potter, T. Morgan, Discovery of sodium and potassium vapor in the atmosphere of the moon, *Science* 241 (4866) (1988) 675–680.
- [13] P.D. Feldman, D. Morrison, The apollo 17 ultraviolet spectrometer: Lunar atmosphere measurements revisited, *Geophys. Res. Lett.* 18 (11) (1991) 2105–2108.
- [14] B. Flynn, S. Stern, A spectroscopic survey of metallic species abundances in the lunar atmosphere, *Icarus* 124 (2) (1996) 530–536.
- [15] A. Potter, T. Morgan, Coronagraphic observations of the lunar sodium exosphere near the lunar surface, *J. Geophys. Res. Planets* 103 (E4) (1998) 8581–8586.
- [16] J.C. Cook, S.A. Stern, P.D. Feldman, G.R. Gladstone, K.D. Retherford, C.C. Tsang, New upper limits on numerous atmospheric species in the native lunar atmosphere, *Icarus* 225 (1) (2013) 681–687.
- [17] M. Benna, P. Mahaffy, J. Halekas, R. Elphic, G. Delory, Variability of helium, neon, and argon in the lunar exosphere as observed by the lafee nms instrument, *Geophys. Res. Lett.* 42 (10) (2015) 3723–3729.
- [18] J. Halekas, M. Benna, P. Mahaffy, R. Elphic, A. Poppe, G. Delory, Detections of lunar exospheric ions by the lafee neutral mass spectrometer, *Geophys. Res. Lett.* 42 (13) (2015) 5162–5169.
- [19] R.R. Hodges, Methane in the lunar exosphere: implications for solar wind carbon escape, *Geophys. Res. Lett.* 43 (13) (2016) 6742–6748.
- [20] C. Grava, K. Retherford, D. Hurley, P. Feldman, G. Gladstone, T. Greathouse, J. Cook, S. Stern, W. Pryor, J. Halekas, et al., Lunar exospheric helium observations of Iro/lamp coordinated with artemis, *Icarus* 273 (2016) 36–44.
- [21] S.A. Stern, The lunar atmosphere: history, status, current problems, and context, *Rev. Geophys.* 37 (4) (1999) 453–491.
- [22] M. Sarantos, R.M. Killen, A.S. Sharma, J.A. Slavin, Influence of plasma ions on source rates for the lunar exosphere during passage through the earth's magnetosphere, *Geophys. Res. Lett.* 35 (4) (2008).
- [23] L. Starukhina, Computer simulation of sputtering of lunar regolith by solar wind protons: contribution to change of surface composition and to hydrogen flux at the lunar poles, *Sol. Syst. Res.* 37 (1) (2003) 36–50.
- [24] L.V. Starukhina, Y.G. Shkuratov, The lunar poles: water ice or chemically trapped hydrogen? *Icarus* 147 (2) (2000) 585–587.
- [25] W.E. Schiesser, *The Numerical Method of Lines: Integration of Partial Differential Equations*, Elsevier, 2012.
- [26] J.F. Ziegler, J.P. Biersack, U. Littmark, The stopping and range of ions in matter, SRIM:<http://www.srim.org>.
- [27] M. Tona, S. Takahashi, K. Nagata, N. Yoshiyasu, C. Yamada, N. Nakamura, S. Ohtani, M. Sakurai, Coulomb explosion potential sputtering induced by slow highly charged ion impact, *Appl. Phys. Lett.* 87 (22) (2005) 224102–224102.
- [28] M. Thompson, II, the energy spectrum of ejected atoms during the high energy sputtering of gold, *Philos. Mag.* 18 (152) (1968) 377–414.
- [29] R.A. Baragiola, Sputtering: survey of observations and derived principles, *Philos. Trans. R. Soc. London Ser. A: Math. Phys. Eng. Sci.* 362 (1814) (2004) 29–53.
- [30] F. Ruan, D. Yu, M. Zhang, W. Wang, J. Chen, Z. Song, X. Cai, Energy spectra of sputtering ions induced by ar<sup>7+</sup>, 9<sup>+</sup> ions on graphite collisions, *J. Phys. Conf. Ser.* vol. 194, IOP Publishing, 2009, p. 132037.
- [31] L. Starukhina, Impact melting of regolith particles by micrometeorites as a mechanism of soil maturation, in: 37th Annual Lunar and Planetary Science Conference, vol. 37, 2006.